


Article

Interannual Variability of Salinity in the Chukchi Sea and Its Relationships with the Dynamics of the East Siberian Current during 1993–2020

Vladislav R. Zhuk *  and Arseny A. Kubryakov 

Federal State Budget Scientific Institution, Marine Hydrophysical Institute of RAS, 299011 Sevastopol, Russia; arskubr@mhi-ras.ru

* Correspondence: zhuk-vladislav@ya.ru

Abstract: The interannual features of the salinity in the Chukchi Sea during the ice-free period of a year are investigated on the base of Soil Moisture Active Passive (SMAP) satellite measurements and GLORYS12v1 reanalysis data. Analysis of salinity measurements revealed two types of Bering Summer Waters (BSW) propagation: “western” and “eastern”. The first is characterized by the penetration of Pacific waters into the northwest part of the sea, as well as the propagation of BSW to 180°W and 72.5°N. During the “eastern” type, salty waters are pressed to the eastern part of the shelf. Their area decreases and the northern boundary of the BSW area shifts to 174–176°W. Areas with low salinity, ~29 psu, are observed in the western part of the sea. Our study reveals that the formation of these types is affected not only by the inflow of Pacific waters through the Bering Strait but also by the East Siberian Current (ESC). Both factors are related and lead to correlated changes in the salinity of the Chukchi Sea waters. ESC carries Arctic freshwaters from west to east and leads to a decrease in salinity in the western part of the sea. At the same time, southward ESC caused the blockage of the northward currents in the Bering Strait and a decrease in the influx of saline Pacific waters in the southern part of the Chukchi Sea. The intensification of ESC occurred in 1994, 2002, 2012, and 2016, when the volume transport of ESC increased by approximately 0.2 Sv, while the influx through the Bering Strait decreased. As a result, in the years with intense ESC, the spatial structure of the salinity of the Chukchi Sea changed significantly and the shelf-averaged salinity decreased by 0.3–0.5 psu.

Keywords: Chukchi Sea; Bering Strait; East Siberian Current; Pacific waters; water masses; seasonal and interannual variability; Arctic Ocean; salinity distribution; salt transport



Citation: Zhuk, V.R.; Kubryakov, A.A. Interannual Variability of Salinity in the Chukchi Sea and Its Relationships with the Dynamics of the East Siberian Current during 1993–2020. *Remote Sens.* **2023**, *15*, 5648. <https://doi.org/10.3390/rs15245648>

Academic Editors: Chung-Ru Ho and Ulrich Kamp

Received: 12 September 2023

Revised: 2 November 2023

Accepted: 1 December 2023

Published: 6 December 2023



Copyright: © 2023 by the authors. Licensee MDPI, Basel, Switzerland. This article is an open access article distributed under the terms and conditions of the Creative Commons Attribution (CC BY) license (<https://creativecommons.org/licenses/by/4.0/>).

1. Introduction

The shallow Chukchi Sea is a gateway for the Pacific waters entering the Arctic Ocean. These waters play an important role in the formation of the freshwater balance of Beaufort Gyre [1], salinity distribution, and the formation of halocline in the eastern Arctic [2]. The transport of salt, heat and nutrients associated with the Pacific waters has a significant impact on the thermohaline structure [3,4], marine ecosystems [5], and melting of sea ice [4,6] in the Chukchi Sea. The average annual volume transport through the Bering Strait is estimated at 0.8 Sv [3,7].

Most of the modern studies are based on the mooring measurements, in the eastern part of the Chukchi Sea [8–11]. The inflowing Pacific Summer Waters consist of several water masses, particularly cold and salty Bering Summer Waters (BSW) and warm, and fresh Alaskan Coastal Waters (ACW), primarily formed from continental runoff into the Gulf of Alaska [5,8]. As a rule, BSW is below ACW [12,13]. Generally, it is believed that Pacific waters progress poleward across the Chukchi shelf by the western pathway through Herald Canyon [12], the Central Channel pathway [14], and the Alaskan Coast [10,11,15].

At the same time, due to the relatively low number of measurements, the water masses distribution and related salinity patterns in the western part of the Chukchi Sea

remain poorly studied. However, several studies [12,16–18] point to the existence of strong interannual variability of these characteristics. For example, Alaskan waters penetrated into the western part of the sea in 2008 and 2009 [16] but were absent in 2004 [12]. Pisareva et al. [16] discovered an unusual configuration of waters in September 2009 based on in situ measurements. The ACW occupied the western part of the Bering Strait in the form of an along-bottom current. Then, ACW headed northwards to the Herald Canyon. At the same time, BSW occupied the eastern part of the Bering Strait. This configuration was caused by strong northeasterly winds leading to Ekman transport of ACW to the western part of the strait. Based on modeling data, Kinney et al. [17] consider that part of Pacific waters moves into the East Siberian Sea through the Long Strait. An increase in BSW by 30% compared to 2008 was detected in the Herald Canyon in 2014 [16]. The analysis of in situ measurements in 2003 and 2007 by Vanin [18] demonstrated the significant impact of Arctic atmospheric circulation on the thermohaline structure of this region. Cyclonic atmospheric circulation is favorable for the eastward transport of relatively cold and fresh masses from the Arctic. Conversely, anticyclonic atmospheric circulation leads to rapid heating of the surface layer, ice melting, and upwelling in the coastal zone under the influence of southern and southeastern winds [18–20]. However, much of the research listed is based on short-term in situ measurements. Many questions regarding the long-term variability of salinity and the propagation of water masses in the western part of the Chukchi Sea remain poorly understood.

In a number of recent publications, it has been noted that the Arctic circulation also significantly affects the flow of Pacific waters through the Bering Strait [21,22]. Under certain atmospheric conditions, a quasi-permanent flow is formed along the coast of the Laptev and East Siberian Seas during the ice-free period, moving eastward [23–26]. This flow carries freshwaters from the Lena River runoff into the Chukchi Sea [26,27]. In some years, the flow can reach the Bering Strait [23] and lead to a significant decrease in the influx of Pacific waters to the Chukchi Sea [28].

Modern satellite salinity measurements give the possibility of investigating the spatial variability of the haline structure of the Arctic Ocean. Particularly, information from these satellites has been used to study the propagation of river plumes [24,29–31], as well as to track the salinity variability of the Bering Sea [32,33]. The latest mission Soil Moisture Active Passive (SMAP) makes it possible to obtain salinity data with a higher spatial resolution and accuracy [32,34]. Validation of these salinity measurements in the Arctic regions has shown good agreement between SMAP satellite products and in situ data (RMSE < 1 psu) [33–35]. In addition to information obtained from the salinity satellite, we also used data from the modern GLORYS12v1 reanalysis. This allows for a relatively accurate description of the vertical distribution and hydrological characteristics of water masses [36,37]. In this study, we use satellite measurements to investigate the interannual changes in the salinity in the Chukchi Sea during an ice-free period. Further, we use GLORYS12v1 data to investigate the causes of interannual changes in the salinity and its impact on the water masses distribution on the shelf.

This paper is structured as follows. Section 2 details the data used from satellite observations, ocean reanalysis and calculating methodology. Section 3 presents the main results. Section 3.1 focuses on the features of the salinity spatial distribution in the Chukchi Sea. Section 3.2 describes the propagation of the main types of Pacific waters and the variability of its extent in the shelf. Section 3.3 displays the results of current analysis in the western part of the sea and demonstrates the influence of the East Siberian Current on the distribution of water masses. Section 4 discusses the outcomes of this work as well as possible errors. Finally, Section 5 summarizes the conclusions of this study.

2. Materials and Methods

2.1. SMAP Data

We used monthly and 8-day running averaged surface salinity maps obtained from measurements of the SMAP instrument for 2015–2020 to study the interannual variability.

The product SMAP sea surface salinity (SSS) V4.0 was downloaded from <http://remss.com/missions/smap/salinity/> accessed on 3 April 2021. The major change in version 4.0 from version 3.0 is an improved land correction, which allows for SMAP salinity retrievals closer to the coast [38]. The dataset has a 0.25° spatial resolution and has been available since July 2015. The estimated SMAP accuracy is approximately 0.5 psu [38]. However, at high latitudes (above 65°N) the accuracy of SSS measurements decreases due to lower sea temperature. Fournier et al. [34] show that in the Arctic Ocean RMSD (root-mean-square deviation), bias, correlation coefficients between SMAP data and in situ salinity measurements are 1.20 psu, -0.16 psu, and 0.93, respectively. Fournier et al. [34] consider that SMAP Remote Sensing Systems (RSS) had a lower RMSD relative to in situ than other SMAP and SMOS products.

2.2. GLORYS12v1 Data

Monthly mean fields of velocity, temperature, and salinity were analyzed using GLORYS12v1 reanalysis data product GLOBAL_REANALYSIS_PHY_001_030 for the period from 1993 to 2019 accessed on 8 December 2021. This reanalysis configuration is based on the global operational system $1/12^\circ$ Mercator Océan [37] using the NEMO3.1 ocean and sea-ice general circulation model with 50 vertical levels and available horizons up to 5900 m. Copernicus Marine Environment Monitoring Service (CMEMS) data from along-track altimetry sea level anomaly (SLA), satellite sea surface temperature (SST), and sea ice concentration are assimilated together with in situ vertical profiles of temperature and salinity (T/S) from the Coriolis Ocean Dataset for Reanalysis (CORA) database [39]. The advantage of the new product compared to previous versions is the possibility to analyze ocean dynamics with a higher resolution. For the global ocean, the average difference between observations does not exceed 0.2 psu and 0.4°C for salinity and temperature, respectively (37). However, the difference can increase in the Arctic (reaches 2.4 psu) [40]. Moreover, in the study [41], in situ measurements in the Barents Sea were compared with reanalysis data, which showed a difference between these data in the form of temperature field anomalies of only approximately 0.7°C .

2.3. Water Masses Definition and Calculation Process

This study investigates the interannual variability of the dominant water masses of the Chukchi Sea: BSW and ACW. Definitions of these water masses based on temperature and salinity parameters were taken from [12]. BSW is defined as waters with temperature ranging from -1 to 3°C and salinity from 30 to 33.3 psu, and ACW as waters with temperature ranging from 3 to 5°C and salinity from 30.5 to 33.3 psu. As noted by Linders et al. [12], these boundaries should be considered approximate, but they are sufficient for our goals and agree with previous studies of the region, e.g., [16,42].

Formulas to calculate water transport (F) and salinity transport (F_s) are defined as:

$$F = V \times s, \quad (1)$$

$$F_s = \rho \times S_w \times F \quad (2)$$

where F and F_s is presented in Sv ($10^6 \text{ m}^3/\text{s}$) and kg/s respectively, V is the average flow velocity in the section (m/s), and s is the cross-sectional area (m^2). S_w is the average salinity in the section. The density (ρ) of seawater was calculated using the TEOS-10 equation of state for seawater (kg/m^3). In particular, we use a Gibbs-SeaWater (GSW) Oceanographic Toolbox [43]. Depth-averaged values are defined as follows. The analysis data are interpolated on a grid with a depth step of 1 m. Then, the average of this grid (in section/area) is calculated. Visualization was performed using the standard Matlab code: "contourfm", "imagesc", "plot", etc.

3. Results

3.1. Interannual Variability of Salinity in the Chukchi Sea

Figure 1a shows a bathymetry map with a study area in the Arctic Ocean. The SMAP data are unavailable for most of the area during winter due to the significant amount of ice in the Chukchi Sea. Therefore, this study investigated the variability of salinity during the ice-free period from July to October. Figure 1b shows the mean map of surface salinity based on SMAP satellite data. It is clearly seen that high-salinity areas (up to 32–33 psu) are located in the southern part of the Chukchi Sea shelf, which is influenced by salty Pacific waters. As the latitude increases, salinity values decrease due to the mixing of Pacific and Arctic waters. In the eastern part of the Chukchi Sea: from the Bering Strait to near the coast of Alaska, there are areas with low-salinity values (~30–31 psu). The decrease in salinity in this area primarily occurs due to the propagation of ACW from the Bering Sea [44]. The greatest drop in salinity (below 24 psu) was observed in the north and associated with ice-melting processes. Figure 1c illustrates the standard deviation map for the salinity of the Chukchi Sea. It can be seen that significant variations in salinity occur 73°N, where values exceed 5 psu. At the same time, substantial variability in the surface salinity distribution is also observed in the western part of the sea—near the coast of the Chukchi Peninsula with comparable standard deviation values.

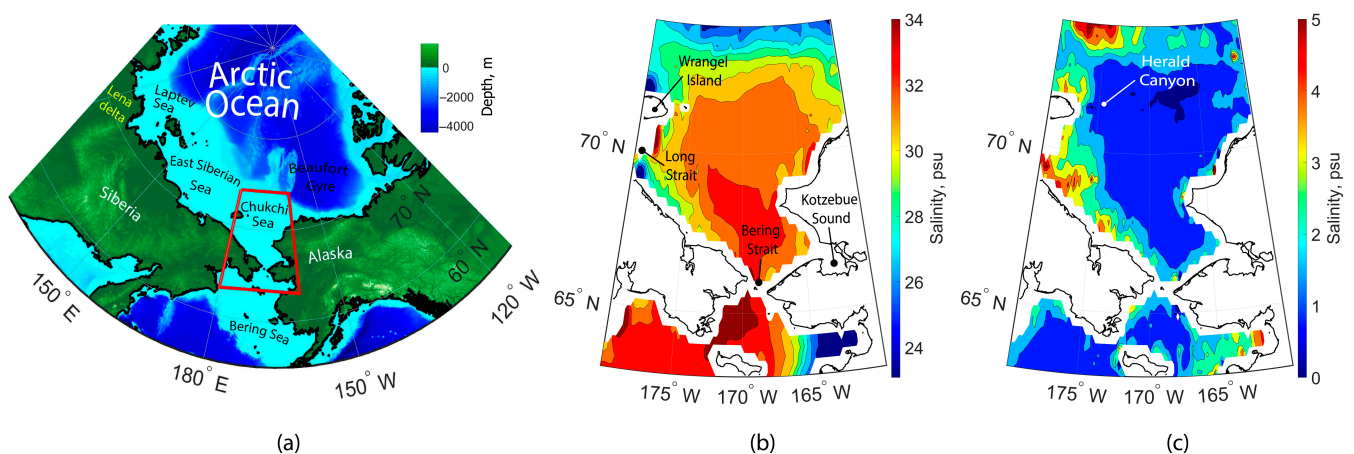


Figure 1. (a) Study area on the bathymetry map. (b) Averaged Sea surface salinity (SSS) and (c) Standard deviation (STD) of sea surface salinity for July–October 2015–2020 based on SMAP data.

Significant interannual variability in the distribution of surface salinity in the Chukchi Sea is observed in Figure 2. We suggest considering two different types based on SSS distribution: “western” and “eastern”. In 2015 and 2020, an elongated area with salinity values of 32–33 psu was observed from the western part of the Bering Strait to 70°N until south of Wrangel Island, defining the “western” type. During the “eastern” type in 2016–2018, the area with high salinity shifted to the east. At the same time, low-salinity areas, with values up to 29–30 psu, are located in the coastal part of the Chukchi Peninsula.

The difference between salinity fields is more clearly visible in Figure 3. It shows maps of anomalies in the mean salinity for each year from the mean salinity field for the entire observation period. The most remarkable feature is the increased anomaly values in 2015. In the central part, values rarely reach 1 psu, while in the western and northern edge of the sea, it ranges from 2 to 3 psu. In 2016, the distribution of anomalies became the opposite: the northern sea part and the waters near the Chukchi coast are covered by negative anomalies (over −3 psu). There are pronounced negative anomalies in the western part of the sea that can be traced in 2017 and 2018, although they are not as widespread as in 2016. In 2019, both positive and negative anomalies were observed. At the same time, the maximum of negative anomalies are located in 170–173°W, which is southeast of the observed increased anomalies along the coast (174–179°W). Thus, we can conclude that, in 2019, both features

of eastern and western types appeared. There is a pronounced “eastern” type with negative salinity regions to the west of the Bering Strait. Increased salinity anomalies are detected south of Wrangel Island, which is remarkable for the “western” type. In 2020, increased salinity anomalies are observed: values ranging from 1.5 to 2.7 psu. They were found at a distance of 100 km from the western coast of Chukchi. The gradual decrease in positive anomalies occurs from the western part of the sea to the northeast.

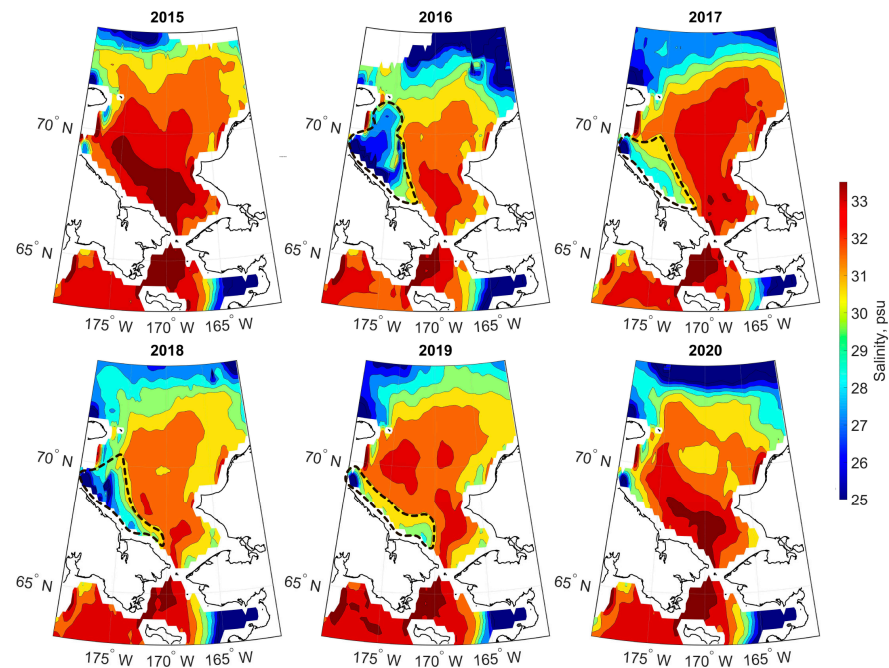


Figure 2. Sea surface salinity (SSS) maps averaged for July–October 2015–2020 based on SMAP data (areas of reduced salinity near to the Chukchi coast are highlighted by black curves).

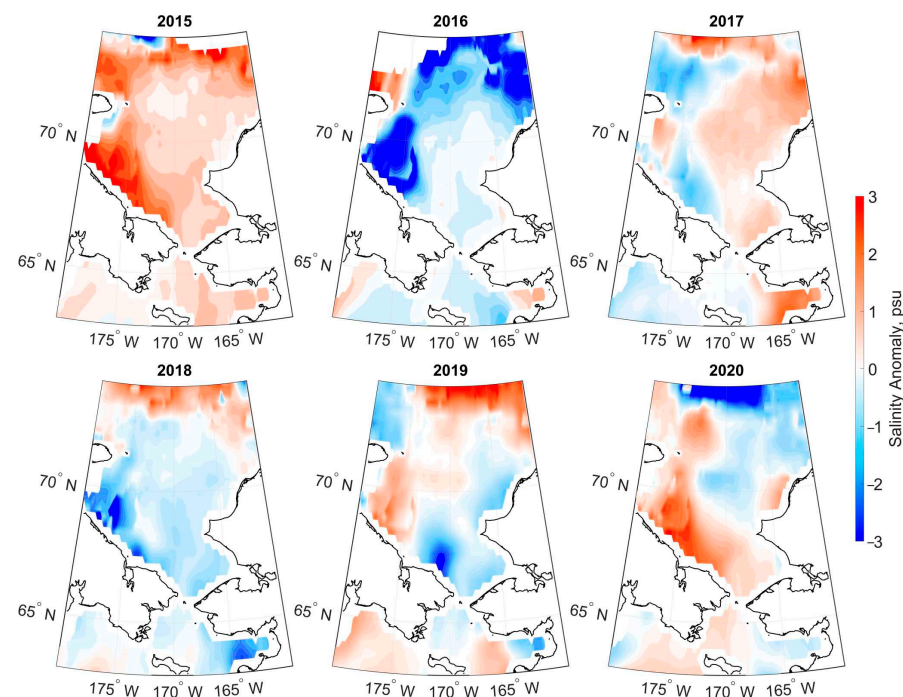


Figure 3. Salinity anomalies maps averaged for July–October 2015–2020 based on SMAP data (averaged for July–October of each year—averaged for July–October of all years).

The SMAP data contain relatively accurate salinity information but have the disadvantage of a limited time series. The GLORYS12v1 reanalysis data for 1993–2019 complement our study. According to satellite data and GLORYS12v1 reanalysis data, two different types of salinity distribution were observed. The “western” type was observed, for example, in 2011, 2014, and 2015 (Figure 4a), when waters with salinity above 31 psu occupied the area from the Bering Strait to nearly 72°N throughout the Chukchi Sea. Areas of low salinity are presented only in the Kotzebue Sound and at higher latitudes, where the influence of ice melting is intensified. Examples of the “eastern” type are noted in 2002, 2012, and 2016 (Figure 4b). In this case, saline waters are shifted eastward, and the maximum salinity does not exceed 31 psu. In the interval from the 180°W meridian and the 31 psu isohaline location, a layer more than 190 km long of low-salinity waters (from 18 to 30 psu) is observed.

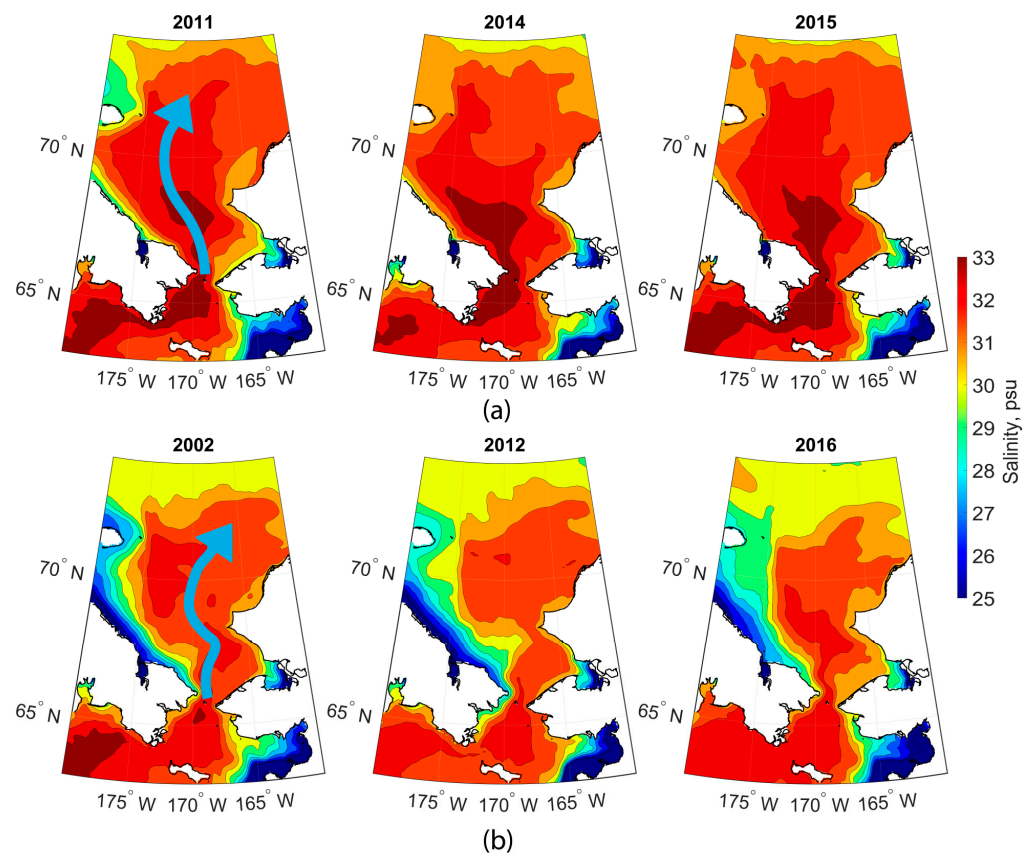


Figure 4. (a) Salinity maps at a depth of 0.5 m averaged for July–October for the “western” type; (b) the same, but for the “eastern” type based on GLORYS12v1 reanalysis data. Arrows indicate the movement of Pacific-origin water with high salinity.

Figure 5 shows the average salinity of the Chukchi Sea. The variability of the mean salinity is generally consistent across different products. In 2016 and 2017, the difference between SMAP and GLORYS12v1 data did not exceed 0.1 psu. The variability dynamics follow a similar pattern over the entire available time range from 2015 to 2019. For example, in 2015, an increased salinity was noticeable in all data, while in 2016, its value decreased. Note that reanalysis data are available at a depth of 0.5 m, while SMAP is available at the sea surface. As can be seen, the features discussed above directly affect the overall salinity of the sea. During the “western” type in 2011 and 2015, the maximum of average salinity is traced both in the depth of 0.5 m and in the depth-averaged variability. In 2002, 2012, and 2016, a decrease of ~1.5 psu and ~0.5 psu was detected at a depth of 0.5 m and in the depth-averaged variability, respectively.

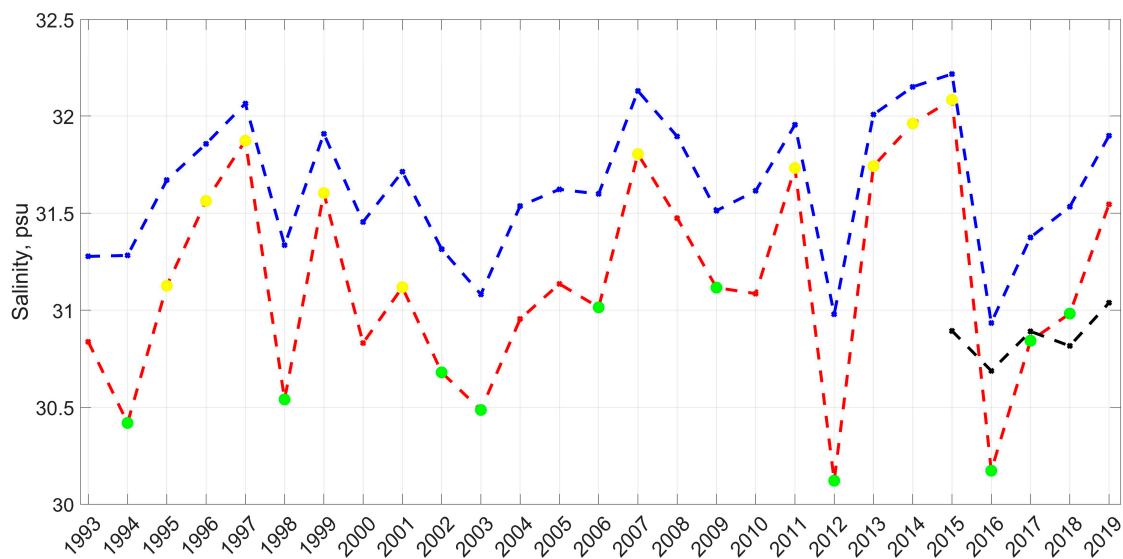


Figure 5. Variability of salinity at a depth of 0.5 m (red curve), depth-averaged salinity (blue curve), and SSS based on SMAP data (black curve), averaged for the period from July to October in the area 163–179°W and 67–72°N. Points indicate “western” (yellow) and “eastern” (green) types based on GLORYS12v1 salinity data. In years without markings, it was not possible to clearly distinguish the predominant type (for details, see the discussion).

3.2. Interannual Variability of the Water Masses Propagation

Figure 6 shows maps of the maximum depth of the relatively cold and saline BSW distribution from July to October based on GLORYS12v1 reanalysis data. These maps illustrate the characteristic areas of BSW propagation in the Chukchi Sea. Similar to the salinity maps, two distinct types of water mass distribution were observed: the “western” type in 1997 and 2015 (Figure 6a,b) and the “eastern” type in 2012 and 2016 (Figure 6c,d). For the “western” type in 2015, the BSW penetrated northward to 73–75°N and occupied the Long Strait at 180°W. BSW occupied almost the entire water column down to 30 m or deeper on the northwestern shelf. In contrast, the 2012 map illustrates that BSW distribution in the western part of the Chukchi Sea was limited to ~174°W. At the same time, a decrease in the penetration of BSW to the north was observed in both 2012 and 2016. For example, in 2016, BSW did not occupy areas north of 72.5°N. However, these waters were present in the Long Strait (up to 25 m) and reached 180°W, but were located farther from the Chukchi Peninsula coast than in 1997 and 2015, when it occupied the entire western coastal area and covered Wrangel Island. Finally, for the “western” type, the most notable difference is the absence of BSW in the central part of the sea. On the other hand, for the “eastern” type, BSW occupied an area in the central part near 68°N 170°W.

Despite the fact that ACW traditionally occupies areas east of BSW and is rarely found in the western part of the shelf, a noticeable difference in the areas of propagation can also be observed for them (Figure 7). In Figure 6a,b in 1997 and 2015, the distribution of ACW is detected throughout the shelf up to 72.5°N. ACW reaches depths of more than 50 m in the extensive central part of the sea. However, it should be noted that, according to ship observations, ACW can be found in the Herald Canyon and the Long Strait quite rarely [11]. There is information that ACW occupied the entire thickness from the surface to the bottom. Also, ACW is simultaneously detected as separate lenses approximately 10 km long at depths from 20 to 30 m [45]. Studying such lenses in detail based on reanalysis data is problematic. However, the main large-scale features coincide with the results obtained from in situ measurements (see, for example, Figure 8 from [45]).

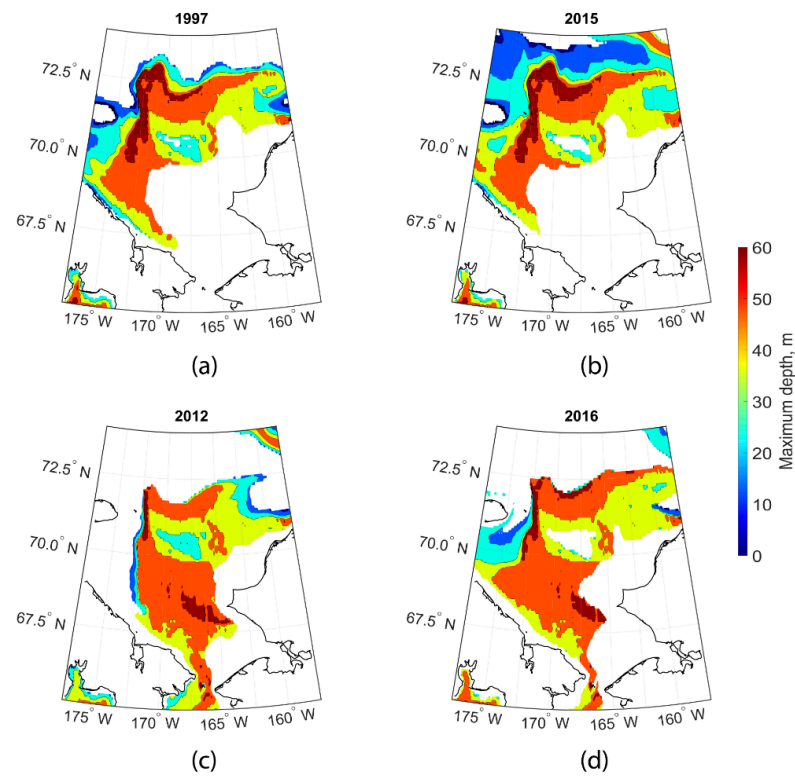


Figure 6. Distribution of maximum depths of BSW averaged for July–October (a) 1997, (b) 2015, (c) 2012, and (d) 2016 based on the GLORYS12v1 reanalysis data for (a,b) “western” and (c,d) “eastern” types. The color indicates the maximum depth occupied by the indicated type of water masses.

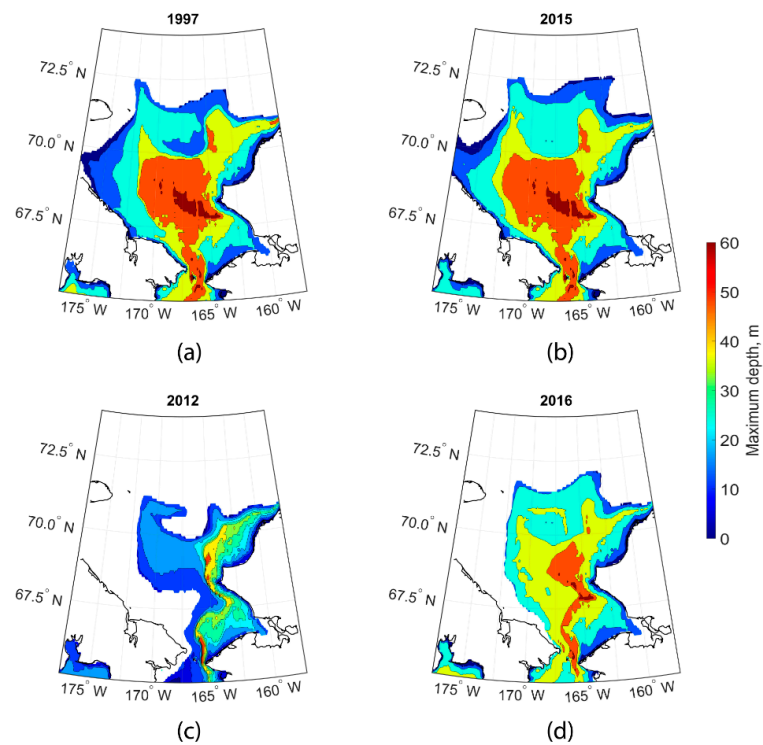


Figure 7. Distribution of maximum depths of ACW averaged for July–October (a) 1997, (b) 2015, (c) 2012, and (d) 2016 based on the GLORYS12v1 reanalysis data for (a,b) “western” and (c,d) “eastern” types. The color indicates the maximum depth occupied by the indicated type of water masses.

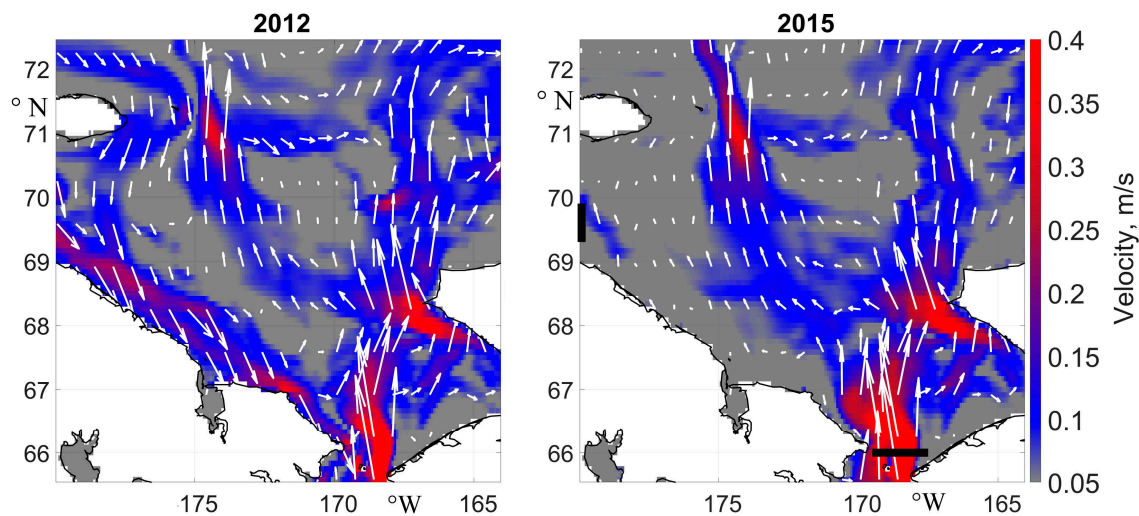


Figure 8. Currents velocity maps at a depth of 0.5 m averaged for the period from July to October for 2012 (left) and 2015 (right). Black lines indicate sections for assessing the dynamics of the Bering Strait and the ESC.

From Figure 7, it can be seen that in years with an “eastern” type, the extent of ACW in the Chukchi Sea is significantly lower than in years with a “western” type. During years with an “eastern” type (Figure 7c,d), there is a significant reduction in the penetration depth of the ACW. At the same time, the boundary of ACW propagation shifts to the east, reaching up to 174–176°W. In particular, in 2012, an even greater displacement of ACW to the east was observed up to 172°W. At a latitude of 67.6°N, the displacement reaches 167°W. ACW occupying depths of more than 35–50 m are observed closer to the Alaska Peninsula and are almost absent in the western part of the sea. At the same time, there is a noticeable decrease in the propagation to the ~71°N.

3.3. Interannual Variability Features of Chukchi Sea Dynamics and Its Influence on Salinity Transport

As can be seen from Figures 2–4, at least two main factors in the Chukchi Sea can cause the differences mentioned above in the water masses propagation. Water flow through the Bering Strait determines the amount of warm and salty water in the western part of the sea and fresher in the eastern part. On the other hand, the propagation of Arctic-origin waters along the coast of Siberia and then along the Chukchi Peninsula determines the volume of fresh and cold water. The salinity maps (Figures 2–4) show that low-salinity areas are well visible in the western part of the sea. In years when the average salinity is reduced both in the depth-averaged variability and on the surface, the eastward transport of Arctic waters may be one of the main reasons for the salinity decrease (Figure 5). This transfer causes a BSW and ACW displacement, which appears in a clearly visible “eastern” type. Although these two factors may be related, incoming waters from the East Siberian Sea may block water exchange through the Bering Strait [28].

Let us consider changes in the circulation structure for the “eastern” 2012 and “western” 2015 types according to GLORYS12v1 data (Figure 8). In 2012, the East Siberian Current is clearly identified. The module of eastward surface currents near the coast of Chukchi reaches 0.2–0.3 m/s in some places. ESC is observed in the form of noticeable southern velocities to the east and south of Wrangel Island with magnitudes up to 0.15 m/s. Velocities in the eastern part of the Bering Strait are directed northward and reach values above 0.4 m/s. However, in the western part, there is a significant weakening of the current and a change in direction towards the south. In 2015, high northward velocities were noticeable across the width of the Bering Strait. The pronounced ESC is absent. On the contrary, there is an increase in northward velocities of Pacific waters originating from

the strait. Currents near Wrangel Island are insignificant (with values less than 0.05 m/s), highlighting the difference in circulation between the two types.

These differences are most noticeable on velocity anomalies maps at a depth of 0.5 m in the western part of the Chukchi Sea (Annual mean minus 1993–2019 mean) (Figure 9). The main feature is the presence of a coastal southeastward current anomaly in 2002, 2012, and 2016 (Figure 9b). The velocity anomaly values reach 0.1 m/s and noticeably differ in the location. For example, in 2012, the width of the area with anomalies above 0.05 m/s was twice as large as in other years. The opposite type was observed in 1999 and 2014–2015, as shown in Figure 9a. During these periods, velocity anomalies directed northwestward were observed in the coastal area of Chukchi Peninsula, indicating a weakening of the ESC. At the same time, anomalies in the Bering Strait are directed northward, indicating an intensification of Pacific flow. These results are consistent with the conclusions of our previous work [28], where on the base of satellite altimetry measurements showed that the ESC and the flow of Pacific waters through the Bering Strait are in anti-phase at monthly scales.

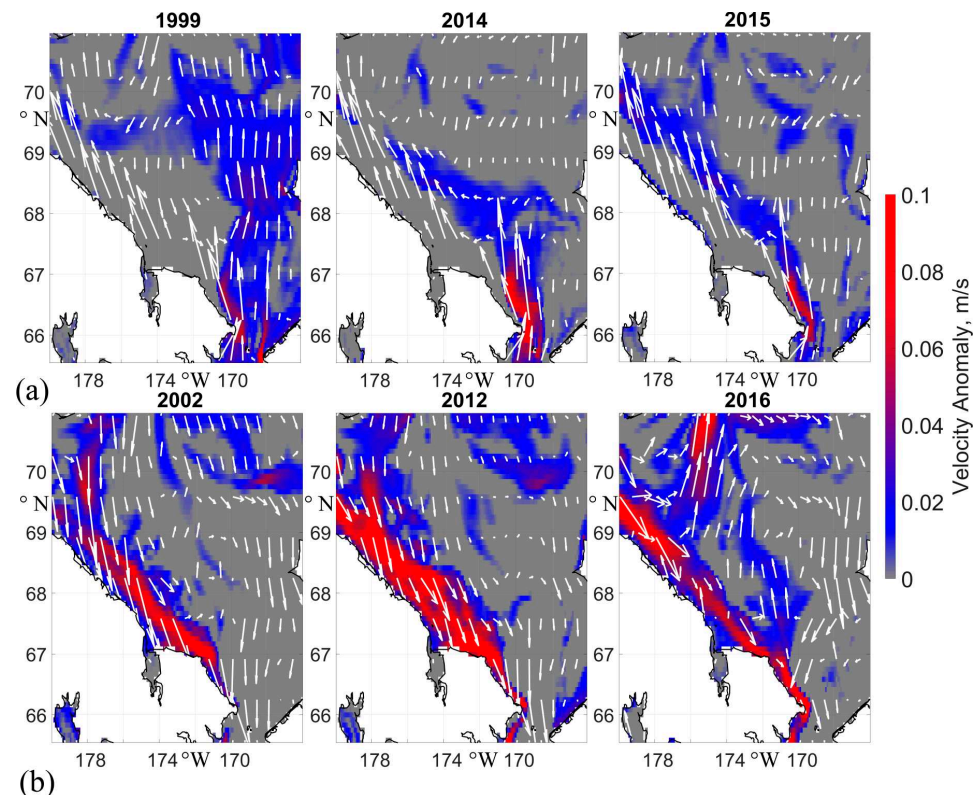


Figure 9. Anomalies of currents velocity maps at a depth of 0.5 m averaged for the period from July to October for (a) 1999, 2014, and 2015 and (b) 2002, 2012, and 2016.

The above maps (Figures 6 and 7) show that the displacement of BSW and ACW occurred during the same periods as the increase in eastern current anomalies near the coast of Chukchi Peninsula, which were clearly observed in 2002, 2012, and 2016. Therefore, the intensification of the ESC serves as an indicator of the reduction in Pacific-origin waters area in the western Chukchi Sea. To evaluate the seasonal and spatial variability of the flow of Pacific waters and ESC, we consider sections along 66°N (Figure 10a) and along 180°W in the Long Strait region (Figure 10b). In agreement with earlier studies [3,7], a maximum of meridional velocities is noted in the Bering Strait from May to August–September, when they exceed 0.5 m/s. At the beginning of the year, there is a decrease in velocity maximum of 0.3–0.4 m/s. There is a decrease in the current velocities down to 0.2 m/s in the

western part of the strait in the region of 168.5–169.5°W from the end of August to the end of November.

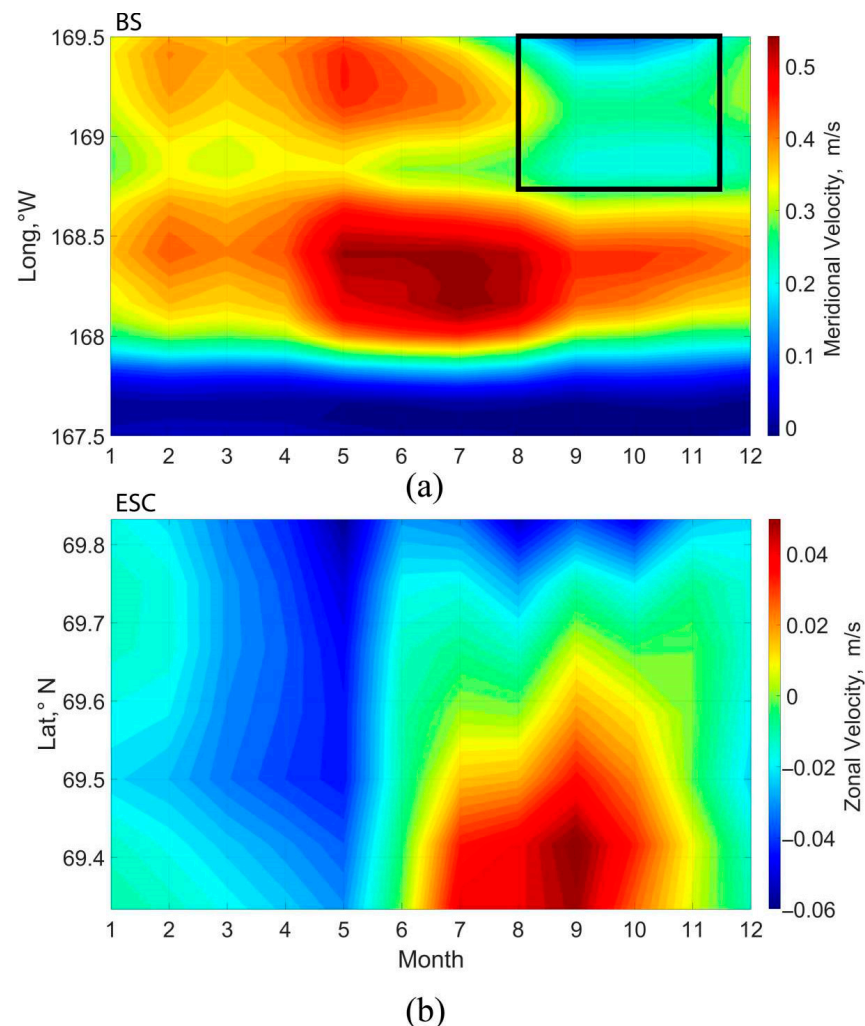


Figure 10. Seasonal depth-averaged variability from 1993 to 2019 of the (a) meridional currents velocity in the zonal section, along 66°N, (positive values indicate northward direction) and (b) zonal currents velocity in the meridional section along 180°W (positive values indicate eastward direction). The black square indicates the area of reduced velocities in the Bering Strait due to the impact of the ESC.

For the ESC section (Figure 10b), maximum western velocities from 0.02 to 0.06 m/s are noted in the winter–spring period. An increase in the zonal component of current velocities in the eastern direction is observed in the ice-free period (from July to October) with values up to 0.04 m/s. This indicates the intensification of water mass transport from the East Siberian Sea to the Chukchi Sea, as well as the increase in the ESC. From September to November, in the Bering Strait, there is a narrow area near 168°45′W–169°30′W (Black square in Figure 10a) with reduced or even zero velocities. This is likely caused by ESC, which increases between July and November. Apparently, ESC affects transport through the strait with a lag time of approximately 1–2 months. However, significant interannual differences in the seasonal cycle of water transport are noted.

Figure 11 shows the seasonal variability of current velocity anomalies for the Bering Strait and the ESC in 2015 and 2016 when opposing types were observed: “western” and “eastern”, respectively. The key differences between the sections are mainly noticeable during the ice-free period. In July–August 2015, northern velocity anomalies were detected in the Bering Strait (Figure 11a). The values reached 0.2 m/s. In September and November,

a decrease in meridional flow is observed. During this time, westward anomalies with values above 0.07 m/s (Figure 11b) are present along the section from mid-June to the end of August. These northern anomalies in the Bering Strait and westward anomalies of the ESC suggest the penetration of Pacific waters into the northwestern part of the Chukchi Sea. Later, in November 2015 (Figure 11b), the sign of the anomaly changed, and values from -0.1 to -0.8 m/s were detected throughout the section. This event occurred simultaneously with southern anomalies in the Bering Strait, highlighting the interrelation of the two currents. The main difference in the Bering Strait in 2016 (Figure 11c) was the presence of southern (negative) velocity anomalies, which lasted from June to September and exceeded -0.2 m/s. At the same time, (Figure 11d), most of the ESC section anomalies had positive values from 0.05 to 0.1 m/s from July to September, indicating an increase in eastern transport. Comparing Figures 11c and 11d, we demonstrate evidence of the relationship between the sections' variabilities. As velocity anomalies increase in the ESC section, a decrease in velocity anomalies can be observed in the Bering Strait. A change in the sign of the anomalies in October was notable and was probably due to a sharp change in the direction and strength of the wind. In August–September, north winds prevailed with a module of no more than 3 m/s south of 72°N . On the contrary, in October a southeast wind direction above 6 m/s was detected (not shown). Note that in 2016, as well as in 2015, there was consistency between the anomaly signs in the two sections for most of the ice-free period.

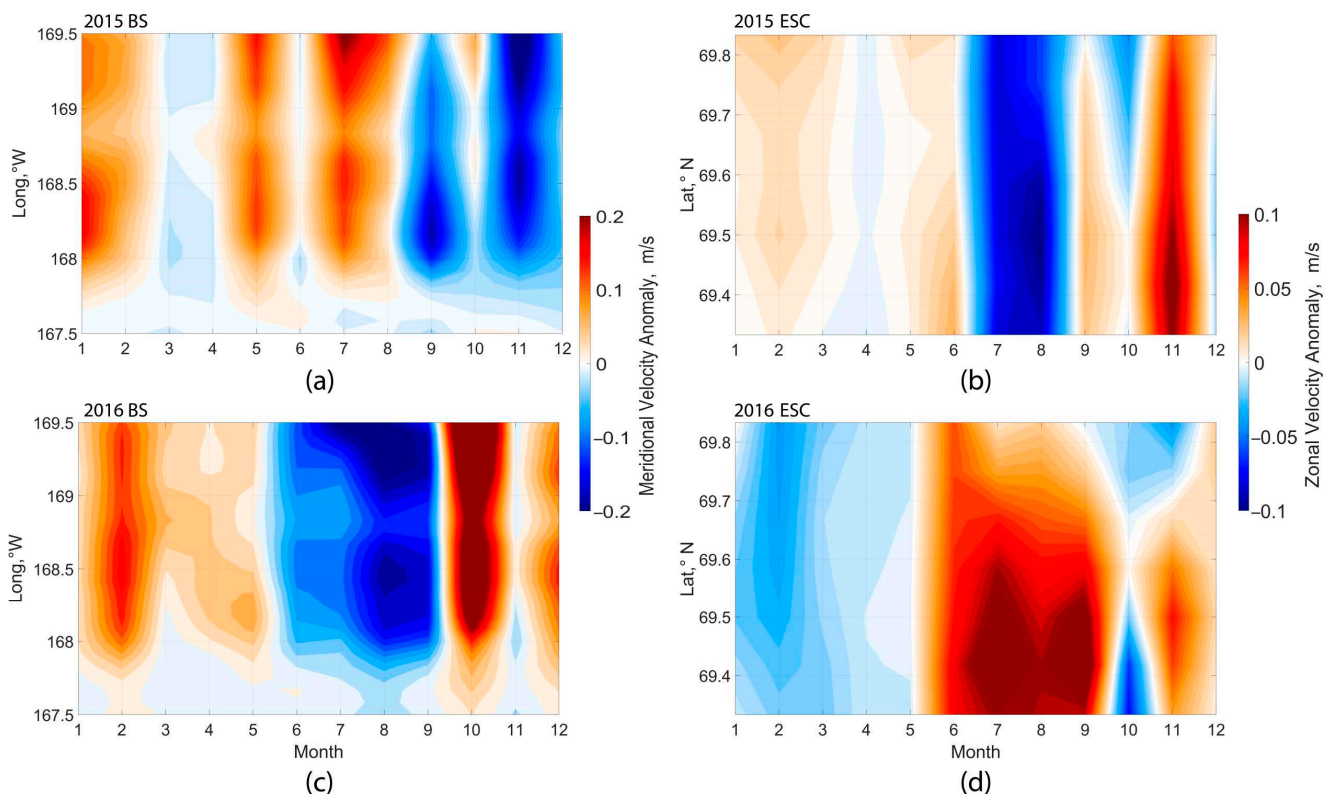


Figure 11. Seasonal depth-averaged variability of the (a,c) meridional currents velocity anomalies in the section along 66°N (positive values indicate northward direction) and (b,d) zonal currents velocity anomalies in the section along 180°W (positive values indicate eastward direction) in (a,b) 2015 and (c,d) 2016.

Figure 12a presents estimates of interannual variability of meridional transport in the Bering Strait (blue dashed line) as well as coastal zonal transport of the ESC. The average transport was 0.77 Sv and 0.04 Sv in the Bering Strait and ESC, respectively. The transport of the ESC (orange dashed line) rarely exceeds 0.1 Sv (Figure 12a). These findings are consistent with studies that reported transport values ranging from 0.1 Sv [23] to 0.3 Sv [16].

Maximum of ESC zonal transport was observed in 1994, 1997, 2001–2003, 2005, 2008, 2012, 2016, and 2018. Among these years, 1994, 2012, and 2016 stood out, with transport to the east increasing by more than 1.5 times relative to other periods. Thus, transport exceeds 0.15 Sv, indicating an intensification of the ESC. During the same years, a weakening of transport in the Bering Strait was detected. For example, in 1994, ESC transport increased by 0.13 Sv (relatively average), while transport in the strait sharply decreased by 0.11 Sv. Similarly 2012, ESC transport increased by 0.2 Sv, while in the strait it was reduced by 0.25 Sv. The minimum of zonal transport was observed in 1995–1996, 1998–1999, 2006–2007, 2011, and 2014–2015, when it reversed to the west with values up to 0.12 Sv. In the same years, northward transport in the Bering Strait increased up to 0.9 Sv and, by 0.13 Sv, relatively of mean value. These results show that changes in the transport of the sections occur in comparable values, which are in accordance with the overall balance of sea transport.

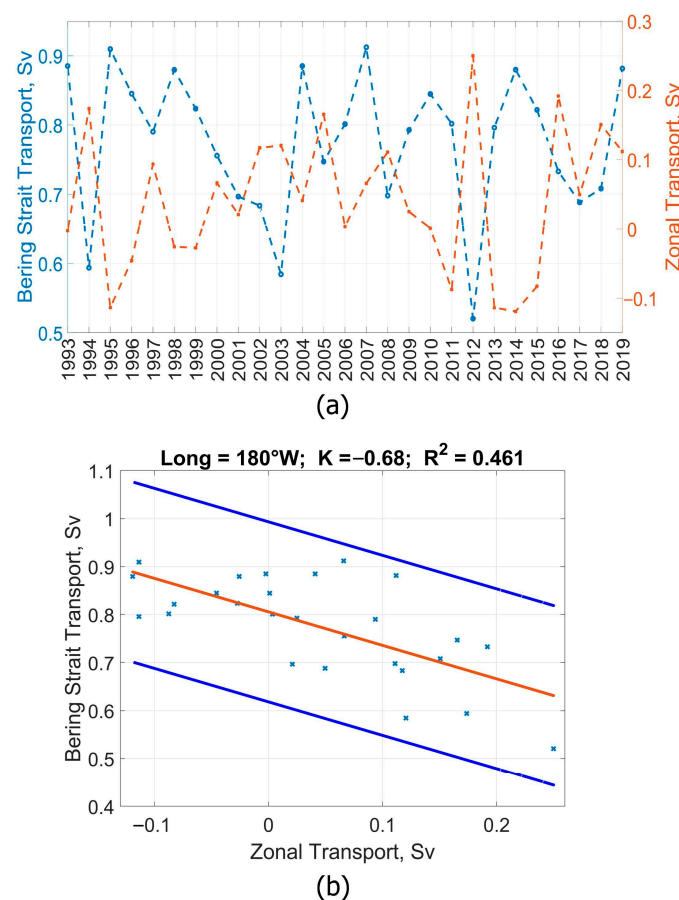


Figure 12. (a) Interannual variability of transport through the Bering Strait in the section along 66°N and the ESC averaged for July–October in the section along 180°W and (b) the scatter diagram between transport in the Bering Strait in the section along 66°N and ESC in the section along 180°W .

Thus, as ESC transport increased (decreased) along the west coast of the Chukchi Peninsula, northward transport in the Bering Strait decreased (increased). The correlation coefficient (K) between variabilities is -0.68 (Figure 12b). The results show that the variability of the ESC is one of the most significant factors in the variability of water transport in the Bering Strait during the ice-free period. This conclusion is consistent with the findings of a recent study [28] obtained from altimetry data.

The graph of interannual variability of salinity transport in the meridional and zonal sections is shown in Figure 13. The transport of salinity is directly related to the volume transport of water, so the features of interannual variability correspond to the results

obtained from the analysis of the volume transport of water. Periods of intensification of the ESC from 3 to 8.3×10^3 kg/s are noted, with a simultaneous decrease in transport through the Bering Strait to 17×10^3 kg/s. Thus, both factors are related and lead to a correlated change in the salinity of the waters of the Chukchi Sea. The ESC transports Arctic freshwaters from west to east, resulting in decreased salinity in the western part of the sea. Simultaneously, there is a decrease in the influx of salty Pacific waters in the southern part of the Chukchi Sea.



Figure 13. Interannual variability of salinity transport through the Bering Strait (in blue) and ESC in the meridional section at 180° W (in orange) averaged for July–October.

4. Discussion

This study investigates the variability of salinity in the Chukchi Sea during the ice-free period from July to October. High-salinity areas are located in the southern part of the shelf, influenced by salty Pacific waters, while low-salinity areas are presented in the coastal part of the Chukchi Peninsula. Significant internal variability in the distribution of SSS based on SMAP data is observed. There are two types of SSS distribution: “western” and “eastern”.

According to the GLORYS12v1 reanalysis data, two types were distinguished in the structure of Pacific-origin waters in the Chukchi Sea. The “western” is characterized by the propagation of BSW almost throughout the shelf, particularly in the northwest part of the Chukchi Sea (up to 180° W and 72.5° N) and penetration into Long Strait and Herald Canyon. The “eastern” differs in reduced propagation both to the north and to the west. A notable indicator is the westward shift of the BSW boundary to 177° W and in some years, even to 175° W (1994, 2012).

The analysis of current velocity anomalies maps showed an increase in the western velocities near the Chukchi coast during the “western” type. Conversely, the eastern anomalies increased during the “eastern” type. The seasonal analysis results for the period from 1993 to 2019 showed that the eastern flow intensifies from July to October, but has significant variations in different years. Interannual anomalies reach 0.06 and 0.1 m/s in the western and eastern directions, respectively. In agreement with recent studies [21,22,28], the interannual dynamics of the Pacific water flow are determined by the sea level field to the north of the Chukchi waters and are related to the East Siberian Sea dynamics.

Features of salinity variability are associated with the impact of the ESC, the intensification of which is driven by wind circulation on the Russian Arctic shelf and the resulting propagation of fresh masses [19,24]. The overall dynamics of these processes determine the density gradients to the north of the Chukchi Sea, forming the sea level field [21,22]. When

the ESC enters the Chukchi Sea, it may change direction from southeast to north and mix with Pacific-origin waters, moving away from the coast [23].

The “western” type is observed in the absence of ESC. In this case, the Arctic circulation and wind forcing favor the penetration of Pacific waters into the western part of the Chukchi Sea. For instance, in 2015, a “northern” type of river plume propagation was observed, caused by eastern winds, which led to the outflow of freshwaters into the central part of the Arctic Basin [24]. This is consistent with the “western” type noted in the Chukchi Sea during this study. We also conclude that the intensification of the ESC is the primary cause of the formation of the “eastern” type. In this case, the type of propagation of freshwater masses from the Laptev and East Siberian Seas is “eastern”, according to our previous work [24]. It is characterized by western winds over the shelf part of the Arctic Basin [26,31]. Thus, intensified ESC displacement BSW away to Alaska, leading to the “eastern” type. Moreover, ESC affects salt transport in the region. Finally, estimates were made for salinity and water transport of the Bering Strait and ESC. The zonal transport to the west in 1995–1996, 1998–1999, 2006–2007, 2011, and 2014–2015 was over 0.1 Sv, and to the east in 1994, 1997, 2001–2003, 2005, 2008, 2012, 2016, and 2018, with the presence of the ESC, it reached 0.24 Sv. These results are in agreement with and complement earlier studies based on in situ measurements [16,23]. The changes in relation to the averaged transports in the two sections are comparable. In 2012, the increase in ESC transport was 0.2 Sv relative to the average. In the same year, the decrease in the Bering Strait transport was 0.25 Sv, which highlights the link between their variability. In the end, the correlation coefficient between the transport of the ESC and the transport in the Bering Strait was 0.68. This demonstrates the significant influence of Arctic waters on the Pacific-origin water mass transport to the Chukchi Sea.

It should be noted that the volume content is influenced by water input in the months prior to the ice-free period. Also, the hydrographic properties can be smoothed out by the monthly average, which can potentially cause the disappearance of BSW in the eastern Chukchi Sea. Also, the water in these areas can be already mixed. Additionally, climatic trends can affect the identification of the water masses as well as unaccounted water types: remnant winter water (WW) and newly ventilated winter water (NVWW). However, these waters are not dominant in the ice-free period and are often observed in the deep-sea part of the sea. The distribution features of ACW and BSW make it possible to distinguish one or another type in most years.

As seen in Figures 2–4, the reanalysis tends to overestimate the values of surface salinity. In addition, it was previously found that GLORYS12v1 demonstrates the smallest salinity gradients compared to other available products [41]. The reanalysis data perform well in the remote zone from the coast but miss much realistic variability near the coastal region and sea ice edge due to a lack of in situ measurements [32].

Ice melting can cause areas of reduced salinity, unrelated to ESC [46]. Therefore, in Figure 5, we did not remark on the type in some years due to the high sea ice concentration (>40%) in the western part of the sea in July. Thus, variability in ice conditions may contribute to the haline characteristics of the shelf. However, most of the ice-melting areas in the ice-free period are located north of the ESC [47]. In recent decades, there was a high sea ice concentration north of 72.5°N even in July. Thus, sea ice influence on the interannual differences in salinity distribution type in this work is relatively small.

5. Conclusions

- (1) Based on SMAP satellite and GLORYS12v1 reanalysis datasets, features of interannual variability of salinity in the Chukchi Sea have been identified. The “western” type is characterized by the penetration of salty waters into the northwestern part of the sea and far into the north covering vast areas in the shelf. The “eastern” type shows a decrease in the area covered by salty waters and freshening of the area near the Chukchi coast. The analysis of calculated maximum depths of BSW and ACW also revealed differences between the two types. During the “western” type, the

propagation of BSW is observed up to 180°W and 72.5°N, with widespread penetration into the Long Strait and Herald Canyon. The main feature of the “eastern” type is the displacement of the western boundary of the BSW area to 174–176°W. Interannual variations in ACW also follow these patterns. Displacement is most noticeable at depths of 5–10 m, where the displacement occurs from ~177°W to 174–175°W.

- (2) There are two main factors that affect the formation of type. Firstly, the inflow of Pacific waters through the Bering Strait. Secondly, the inflow of Arctic-origin waters, which increases during the intensification of the East Siberian Current (ESC). An increase in the average seasonal anomalies of the ESC velocity was detected during the same years when an eastern type was observed with values above 0.1 m/s. On the other hand, opposite anomalies were observed during the western type. The zonal transport of the ESC has varied significantly during 1993–2019, with maxima observed in 1994, 2012, and 2016 up to 0.24 Sv (by 0.2 Sv relative to the average). In the same years, the weakening of transport down to 0.52 Sv (by 0.25 Sv relative to the average) in the Bering Strait was observed. This result is consistent with the transport balance of the Chukchi Sea. The minimum of ESC transport was detected in 1995–1996, 1998–1999, 2006–2007, 2011, and 2014–2015, when it reversed to the west. Therefore, ESC salinity transport intensification reaches up to $3\text{--}8.3 \times 10^3$ kg/s at the same years as water transport due to their similar variability.

A link between these two factors has been confirmed: as the ESC becomes stronger, the transport of water and salinity decreases in the Bering Strait ($K = 0.68$). The variability of the ESC is a significant factor in the variability of water and salinity transport in the Bering Strait during the ice-free period. Thus, a strong ESC causes the “western” type, while its absence is the reason for the “eastern” type.

Author Contributions: Conceptualization, V.R.Z. and A.A.K.; methodology, V.R.Z.; formal analysis, V.R.Z.; investigation, V.R.Z. and A.A.K.; writing—original draft preparation, V.R.Z.; writing—review and editing, A.A.K.; visualization, V.R.Z.; supervision, A.A.K. All authors have read and agreed to the published version of the manuscript.

Funding: This research was funded by the Russian Science Foundation, grant number 21-17-00278, <https://rscf.ru/project/21-17-00278/> (accessed on 3 December 2023).

Data Availability Statement: Satellite data used in this study are freely available. SMAP sea surface salinity (SSS) V4.0 dataset was downloaded from <http://remss.com/missions/smap/salinity/> accessed on 3 April 2021. The GLORYS12v1 reanalysis data (product identifier: GLOBAL_REANALYSIS_PHY_001_030) was obtained from the Copernicus Marine Environmental Monitoring Service (CMEMS) https://data.marine.copernicus.eu/product/GLOBAL_MULTIYEAR_PHY_001_030/services accessed on 8 December 2021.

Conflicts of Interest: The authors declare no conflict of interest.

References

1. Pickart, R.S.; Spall, M.A.; Mathis, J.T. Dynamics of upwelling in the Alaskan Beaufort Sea and associated shelf-basin fluxes. *Deep Sea Res. Part I Oceanogr. Res. Pap.* **2013**, *76*, 35–51. [\[CrossRef\]](#)
2. Timmermans, M.-L.; Marshall, J. Understanding Arctic Ocean circulation: A review of ocean dynamics in a changing climate. *J. Geophys. Res. Oceans* **2020**, *125*, e2018JC014378. [\[CrossRef\]](#)
3. Woodgate, R.A.; Aagaard, K.; Weingartner, T. Monthly temperature, salinity, and transport variability of the Bering Strait through flow. *Geophys. Res. Lett.* **2005**, *32*, L04601. [\[CrossRef\]](#)
4. Serreze, M.C.; Crawford, A.D.; Stroeve, J.C.; Barrett, A.P.; Woodgate, R.A. Variability, trends, and predictability of seasonal sea ice retreat and advance in the Chukchi Sea. *J. Geophys. Res. Oceans* **2016**, *121*, 7308–7325. [\[CrossRef\]](#)
5. Danielson, S.L.; Eisner, L.; Ladd, C.; Mordy, C.; Sousa, L.; Weingartner, T.J. A comparison between late summer 2012 and 2013 water masses, macronutrients, and phytoplankton standing crops in the northern Bering and Chukchi Seas. *Deep Sea Res. Part II Top. Stud. Oceanogr.* **2017**, *135*, 7–26. [\[CrossRef\]](#)
6. Woodgate, R.A.; Weingartner, T.; Lindsay, R. The 2007 Bering Strait oceanic heat flux and anomalous Arctic sea-ice retreat. *Geophys. Res. Lett.* **2010**, *37*, L01602. [\[CrossRef\]](#)
7. Woodgate, R.A. Increases in the Pacific inflow to the Arctic from 1990 to 2015, and insights into seasonal trends and driving mechanisms from year-round Bering Strait mooring data. *Prog. Oceanogr.* **2018**, 124–154. [\[CrossRef\]](#)

8. Corlett, W.B.; Pickart, R.S. The Chukchi slope current. *Prog. Oceanogr.* **2017**, *153*, 50–65. [\[CrossRef\]](#)
9. Ovall, B.; Pickart, R.S.; Lin, P.; Stabeno, P.; Weingartner, T.; Itoh, M.; Kikuchi, T.; Dobbins, E.; Bell, S. Ice, wind, and water: Synoptic-scale controls of circulation in the Chukchi Sea. *Prog. Oceanogr.* **2021**, *199*, 102707. [\[CrossRef\]](#)
10. Itoh, M.; Pickart, R.S.; Kikuchi, T.; Fukamachi, Y.; Ohshima, I.K.; Simizu, D.; Arrigo, K.; Vagle, S.; He, J.; Ashjian, C.; et al. Water properties, heat and volume fluxes of Pacific water in Barrow Canyon during summer 2010. *Deep Sea Res. Part I Oceanogr. Res. Pap.* **2015**, *102*, 43–54. [\[CrossRef\]](#)
11. Stabeno, P.; Kachel, N.; Ladd, C.; Woodgate, R. Flow patterns in the eastern Chukchi Sea: 2010–2015. *J. Geophys. Res. Oceans* **2018**, *123*, 1177–1195. [\[CrossRef\]](#)
12. Linders, J.; Pickart, R.S.; Björk, G.; Moore, G.W.K. On the nature and origin of water masses in Herald Canyon, Chukchi Sea: Synoptic surveys in summer 2004, 2008, and 2009. *Prog. Oceanogr.* **2017**, *159*, 99–114. [\[CrossRef\]](#)
13. Kodryan, K.V.; Kivva, K.K.; Zubarevich, V.L.; Pedchenko, A.P. Water Masses in the Western Chukchi Sea in August 2019 and Their Hydrochemical Features. *Oceanology* **2023**, *63*, 314–324. [\[CrossRef\]](#)
14. Weingartner, T.; Aagaard, K.; Woodgate, R.; Danielson, S.; Sasaki, Y.; Cavalieri, D. Circulation on the north central Chukchi Sea shelf. *Deep Sea Res. Part II Top. Stud. Oceanogr.* **2005**, *52*, 3150–3174. [\[CrossRef\]](#)
15. Lin, P.; Pickart, R.S.; Våge, K.; Li, J. Fate of warm Pacific water in the Arctic basin. *Geophys. Res. Lett.* **2021**, *48*, e2021GL094693. [\[CrossRef\]](#)
16. Pisareva, M.; Pickart, R.; Spall, M.; Nobre, C.; Torres, D.J.; Moore, G.W.K.; Whitley, E.T. Flow of pacific water in the western Chukchi SEA: Results from the 2009 RUSALCA expedition. *Deep Sea Res. Part I Oceanogr. Res. Pap.* **2015**, *105*, 53–73. [\[CrossRef\]](#)
17. Kinney, C.J.; Assmann, K.M.; Maslowski, W.; Björk, G.; Jakobsson, M.; Jutterström, S.; Lee, Y.J.; Osinski, R.; Semi-letov, I.; Ulfso, A.; et al. On the circulation, water mass distribution, and nutrient concentrations of the western Chukchi Sea. *Ocean Sci.* **2022**, *18*, 29–49. [\[CrossRef\]](#)
18. Vanin, N.S. Thermohaline water structure on the southwestern Chukchi Sea shelf under conditions of opposite regimes of atmospheric circulation in summer periods of 2003 and 2007. *Russ. Meteorol. Hydrol.* **2010**, *35*, 468–475. [\[CrossRef\]](#)
19. Dmitrenko, I.A.; Kirillov, S.A.; Krumpfen, T.; Makhotin, M.; Abrahamsen, E.P.; Willmes, S.; Bloshkina, E.; Holemann, J.A.; Kassens, H.; Wegner, C. Wind-driven diversion of summer river runoff preconditions the Laptev Sea coastal polynya hydrography: Evidence from summer-to-winter hydrographic records of 2007–2009. *Cont. Shelf Res.* **2010**, *30*, 1656–1664. [\[CrossRef\]](#)
20. Proshutinsky, A.; Dukhovskoy, D.; Timmermans, M.-L.; Krishfield, R.; Bamber, J.L. Arctic circulation regimes. *Phil. Trans. R. Soc. A* **2015**, *373*, 20140160. [\[CrossRef\]](#)
21. Nguyen, A.T.; Woodgate, R.A.; Heimbach, P. Elucidating Large-Scale Atmospheric Controls on Bering Strait Throughflow Variability Using a Data-Constrained Ocean Model and Its Adjoint. *J. Geophys. Res. Oceans* **2020**, *125*, e2020JC016213. [\[CrossRef\]](#)
22. Peralta-Ferriz, C.; Woodgate, R.A. The Dominant Role of the East Siberian Sea in Driving the Oceanic Flow Through the Bering Strait—Conclusions From GRACE Ocean Mass Satellite Data and In Situ Mooring Observations Between 2002 and 2016. *Geophys. Res. Lett.* **2017**, *44*, 11472–11481. [\[CrossRef\]](#)
23. Weingartner, T.J.; Danielson, S.L.; Sasaki, Y.; Pavlov, V.; Kulakov, M.Y. The Siberian Coastal Current: A wind- and buoyancy-forced Arctic coastal current. *J. Geophys. Res. Oceans* **1999**, *104*, 29697–29713. [\[CrossRef\]](#)
24. Zhuk, V.R.; Kubryakov, A.A. Interannual Variability of the Lena River Plume Propagation in 1993–2020 during the Ice-Free Period on the Base of Satellite Salinity, Temperature, and Altimetry Measurements. *Remote Sens.* **2021**, *13*, 4252. [\[CrossRef\]](#)
25. Wang, X.; Zhao, J.; Lobanov, V.B.; Kaplunenko, D.; Rudykh, Y.N.; He, Y.; Chen, X. Distribution and Transport of Water Masses in the East Siberian Sea and Their Impacts on the Arctic halocline. *J. Geophys. Res. Oceans* **2021**, *126*, e2020JC016523. [\[CrossRef\]](#)
26. Osadchiv, A.A.; Pisareva, M.N.; Spivak, E.A.; Shchuka, S.A.; Semiletov, I.P. Freshwater transport between the Kara, Laptev, and East-Siberian seas. *Sci. Rep.* **2020**, *10*, 13041. [\[CrossRef\]](#) [\[PubMed\]](#)
27. Munchow, A.; Weingartner, T.J.; Cooper, L.W. The summer hydrography and surface circulation of the East Siberian Shelf Sea. *J. Phys. Oceanogr.* **1999**, *29*, 2167–2182. [\[CrossRef\]](#)
28. Zhuk, V.R.; Kubryakov, A.A. Effect of the East Siberian Current on Water Exchange in the Bering Strait Based on Satellite Altimetry Measurements. *Oceanology* **2021**, *61*, 791–802. [\[CrossRef\]](#)
29. Andreev, A.G. The distribution of the desalinated waters of the Amur estuary in the Okhotsk Sea according to satellite observations. *Issled. Zemli Kosmosa* **2019**, *2*, 89–96. (In Russian) [\[CrossRef\]](#)
30. Kubryakov, A.A.; Stanichny, S.V.; Zatsepin, A.G. River plume dynamics in the Kara Sea from altimetry-based lagrangian model, satellite salinity and chlorophyll data. *Remote Sens. Environ.* **2016**, *176*, 177–187. [\[CrossRef\]](#)
31. Tarasenko, A.; Supply, A.; Kusse-Tiuz, N.; Ivanov, V.; Makhotin, M.; Tournadre, J.; Chapron, B.; Boutin, J.; Kolodziejczyk, N.; Reverdin, G. Properties of surface water masses in the Laptev and the East Siberian seas in summer 2018 from in situ and satellite data. *Ocean Sci.* **2021**, *17*, 221–247. [\[CrossRef\]](#)
32. Zhao, J.; Wang, Y.; Liu, W.; Bi, H.; Cokelet, E.D.; Mordy, C.W.; Lawrence-Slavas, N.; Meinig, C. Sea Surface Salinity Variability in the Bering Sea in 2015–2020. *Remote Sens.* **2022**, *14*, 758. [\[CrossRef\]](#)
33. Vazquez-Cuervo, J.; Gentemann, C.; Tang, W.; Carroll, D.; Zhang, H.; Menemenlis, D.; Gomez-Valdes, J.; Bouali, M.; Steele, M. Using Saildrones to Validate Arctic Sea Surface Salinity from the SMAP Satellite and from Ocean Models. *Remote Sens.* **2021**, *13*, 831. [\[CrossRef\]](#)
34. Fournier, S.; Lee, T.; Tang, W.; Steele, M.; Olmedo, E. Evaluation and Intercomparison of SMOS, Aquarius, and SMAP Sea Surface Salinity Products in the Arctic Ocean. *Remote Sens.* **2019**, *11*, 3043. [\[CrossRef\]](#)

35. Tang, W.; Yueh, S.; Yang, D.; Fore, A.; Hayashi, A.; Lee, T.; Fournier, S.; Holt, B. The Potential and Challenges of Using Soil Moisture Active Passive (SMAP) Sea Surface Salinity to Monitor Arctic Ocean Freshwater Changes. *Remote Sens.* **2018**, *10*, 869. [CrossRef]
36. Jean-Michel, L.; Eric, G.; Romain, B.-B.; Gilles, G.; Angélique, M.; Marie, D.; Clement, B.; Mathieu, H.; Olivier, L.G.; Charly, R.; et al. The Copernicus Global 1/12° Oceanic and Sea Ice GLORYS12 Reanalysis. *Front. Earth Sci.* **2021**, *9*, 698876. [CrossRef]
37. Lellouche, J.-M.; Greiner, E.; Le Galloudec, O.; Garric, G.; Regnier, C.; Drevillon, M.; Benkiran, M.; Testut, C.-E.; Bourdalle-Badie, R.; Gasparin, F.; et al. Recent updates on the copernicus marine service global ocean monitoring and forecasting real-time 1/12° high-resolution system. *Ocean Sci.* **2018**, *14*, 1093–1126. [CrossRef]
38. Meissner, T.; Wentz, F.J.; Manaster, A.; Lindsle, R. *Remote Sensing Systems SMAP Ocean Surface Salinities [Level 2C, Level 3 Running 8-day, Level 3 Monthly], Version 4.0 Validated Release*; Remote Sensing Systems: Santa Rosa, CA, USA, 2019. [CrossRef]
39. Cabanes, C.; Grouazel, A.; von Schuckmann, K.; Hamon, M.; Turpin, V.; Coatanoan, C.; Paris, F.; Guinehut, S.; Boone, C.; Ferry, N.; et al. The CORA dataset: Validation and diagnostics of in-situ ocean temperature and salinity measurements. *Ocean Sci.* **2013**, *9*, 1–18. [CrossRef]
40. Hall, S.B.; Subrahmanyam, B.; Morison, J.H. Intercomparison of Salinity Products in the Beaufort Gyre and Arctic Ocean. *Remote Sens.* **2022**, *14*, 71. [CrossRef]
41. Zimin, A.V.; Atadzhanova, O.A.; Konik, A.A.; Gordeeva, S.M. Comparison of Hydrography Observations with Data of Global Products in the Barents Sea. *Fundam. Prikl. Gidrofiz.* **2020**, *13*, 66–77. (In Russian) [CrossRef]
42. Danielson, S.L.; Weingartner, T.J.; Hedstrom, K.S.; Aagaard, K.; Woodgate, R.; Curchitser, E.; Stabeno, P.J. Coupled wind-forced controls of the Bering-Chukchi shelf circulation and the Bering Strait throughflow: Ekman transport, continental shelf waves, and variations of the Pacific-Arctic sea surface height gradient. *Prog. Oceanogr.* **2014**, *125*, 40–61. [CrossRef]
43. McDougall, T.J.; Barker, P.M. Getting Started with TEOS-10 and the Gibbs Seawater (GSW) Oceanographic Toolbox, 2011; 28p. SCOR/IAPSO WG127. Available online: https://www.teos-10.org/pubs/Getting_Started.pdf (accessed on 15 September 2022).
44. Paquette, R.G.; Bourke, R.H. Temperature fine structure near the Sea-ice margin of the Chukchi Sea. *J. Geophys. Res. Oceans* **1979**, *84*, 1155–1164. [CrossRef]
45. Pisareva, M.N.; Pickart, R.S.; Iken, K.; Ershova, E.A.; Grebmeier, J.M.; Cooper, L.W.; Bluhm, B.A.; Nobre, C.; Hopcroft, R.R.; Hu, H.; et al. The Relationship Between Patterns of Benthic Fauna and Zooplankton in the Chukchi Sea and Physical Forcing. *Oceanography* **2015**, *28*, 68–83. [CrossRef]
46. Supply, A.; Boutin, J.; Kolodziejczyk, N.; Reverdin, G.; Lique, C.; Vergely, J.-L.; Perrot, X. Meltwater Lenses Over the Chukchi and the Beaufort Seas During Summer 2019: From In Situ to Synoptic View. *J. Geophys. Res. Oceans* **2022**, *127*, e2021JC018388. [CrossRef]
47. Jay, V.C.; Fischbach, S.A.; Kochnev, A.A. Walrus areas of use in the Chukchi Sea during sparse sea ice cover. *Mar. Ecol. Prog. Ser.* **2012**, *468*, 1–13. [CrossRef]

Disclaimer/Publisher’s Note: The statements, opinions and data contained in all publications are solely those of the individual author(s) and contributor(s) and not of MDPI and/or the editor(s). MDPI and/or the editor(s) disclaim responsibility for any injury to people or property resulting from any ideas, methods, instructions or products referred to in the content.